Core–Valence-Luminescence Cs–M–Cl (M = Zn, Mg) Scintillators for Photon-Counting X-ray Detectors

van Blaaderen, J.J.; Rutstrom, Daniel; Bangoyina, G.; Stand, Louis; van Aarle, C.; de Haas, J.T.M.; Schaart, D.R.; Melcher, Charles L.; Zhuravleva, Maria; Dorenbos, P.

Publication date
2025

Document Version
Final published version

Published in
ACS Applied Optical Materials

ACS APPLIED OPTICAL MATERIALS

pubs.acs.org/acsaom

Article

Core–Valence-Luminescence Cs–M–Cl (M = Zn, Mg) Scintillators for Photon-Counting X-ray Detectors

J. Jasper van Blaaderen,* Daniel Rutstrom, Giles Bangoyina, Luis Stand, Casper van Aarle, Johan de Haas, Dennis R. Schaart, Charles L. Melcher, Mariya Zhuravleva, and Pieter Dorenbos*

Cite This: ACS Appl. Opt. Mater. 2025, 3, 2101–2110

Read Online

ACCESS | Metrics & More | Article Recommendations | Supporting Information

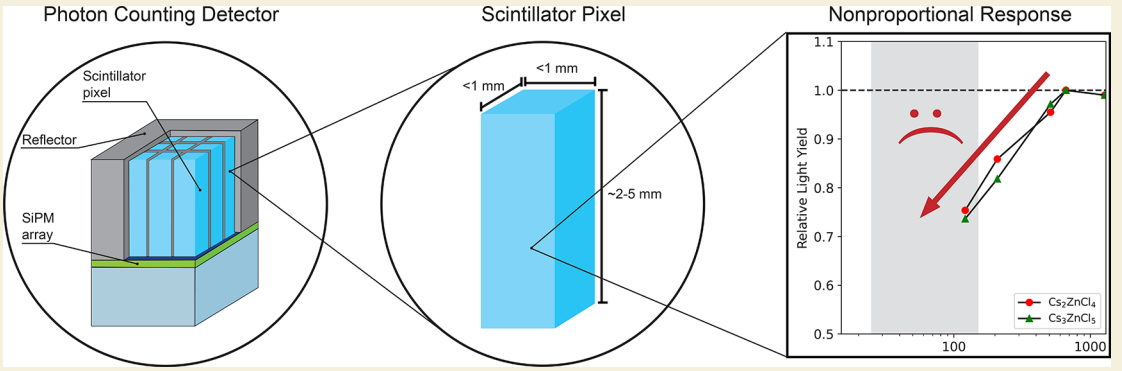

ABSTRACT: X-ray photon-counting detectors (PCDs) are a rapidly developing technology used in medical imaging. Current PCDs are based on room-temperature semiconductors, such as CdTe and CZT, directly converting incident X-ray photons into electrical pulses. An alternative to this approach is the use of ultrafast scintillators in combination with silicon photomultipliers. A very interesting class of materials potentially suitable for this application is scintillators exhibiting core–valence luminescence (CVL), which typically has a decay time between 0.5 and 2 ns. In this work, two families of Cs–Cl-based compounds, Cs–Zn–Cl and Cs–Mg–Cl, are investigated for their potential application in PCDs. These families of compounds are especially interesting because most members exclusively show CVL at room temperature, resulting in a fast scintillation pulse containing no slow components. Additionally, several approaches to tailor the scintillation properties of these materials, i.e., doping with Br^- and Zn^{2+}, are studied. Unfortunately, all compounds show a strong drop in the CVL response in the diagnostic energy range (25–150 keV), the operational range of a PCD. PCDs based on these materials will thus be able to handle the high X-ray fluence rate of an imaging task but will not be able to sufficiently discriminate the energies of incident X-ray photons. In addition to the Cs–Zn–Cl and Cs–Mg–Cl compounds, the nonproportional response of the CVL component of BaF_2 is studied utilizing fast digitization of individual scintillation pulses in order to discriminate between processes related to the CVL and self-trapped exciton emission of BaF_2.

KEYWORDS: *core–valence luminescence, scintillators, photon-counting detectors, photon-counting computed tomography, halide scintillators, nonproportional response*

1. INTRODUCTION

X-ray computed tomography (CT) is one of the most commonly used medical imaging techniques. Current CT systems are often based on energy integrating detectors (EIDs), which are limited in spatial resolution, and the contrast-to-noise ratio for a given radiation dose.[1,2] These limitations could be mitigated by moving from EIDs to photon-counting X-ray detectors (PCDs).[2−6] This results from the fact that a PCD detects the number of incident X-ray photons and assigns them to an energy bin, discriminating incident X-ray photons with different energies. This requires that PCDs not only handle the high incident X-ray photon fluence rates of an imaging task but also have sufficient energy resolution.

Current PCD-based CT scanners utilize the direct conversion of the energy of the incident X-ray photons into electrical pulses using room-temperature semiconductors like CdTe,[7,3] CdZnTe,[8,3] or Si.[9,10] These semiconductor-based detectors can be referred to as direct PCDs. Unfortunately, direct PCDs face two major drawbacks: the cost of producing high-quality semiconductor crystals and the poor signal-to-

Received: July 2, 2025
Revised: August 26, 2025
Accepted: August 26, 2025
Published: September 1, 2025

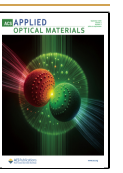

https://doi.org/10.1021/acsaom.5c00253
ACS Appl. Opt. Mater. 2025, 3, 2101–2110

noise ratio.[1,11,12] An alternative, addressing these challenges, is to switch from direct PCDs to indirect PCDs, i.e., utilizing fast scintillators coupled to fast silicon photomultipliers (SiPMs).[12] In our recent work, ref 24, we have presented a general framework for the assessment of different types of scintillators in a SiPM-based indirect PCD, taking into account the properties of both the scintillator and the SiPM. The ideal scintillator should have a short decay time, with a negligible rise time, in order to deal with the high incident X-ray photon fluence rate of an imaging task. Additionally, such a scintillator should have sufficient energy resolution in the diagnostic energy range (25−150 keV), necessary to discriminate between different incident X-ray energies.

Only a few scintillators have been explored experimentally for their use in indirect PCDs. Van der Sar et al. studied the performance of $LaBr_3:Ce^{3+}$, which has a decay time of 16 ns,[13] coupled to SiPMs with a recharge time of 7 ns.[14−17] Additionally, several garnet-based scintillators have been explored, for example, by Arimoto et al., Sato et al., and Shimazoe et al., showing encouraging results for indirect PCD CT.[12,18−22] One of the down sides of these garnet-based indirect PCDs however is their decay time in the range of 50−70 ns, restricting the fluence rate conditions. Another type of scintillator we explored in our previous work, ref 23, is the hybrid organic−inorganic compound $(BZA)_2PbBr_4$, which has a decay time of 4.2 ns. One of the downsides of this material, however, is its low density (2.23 g/cm^3).

An interesting type of fast scintillators not yet studied for this application are materials exhibiting core−valence luminescence (CVL), sometimes also referred to as cross-luminescence.[25] CVL typically exhibits a decay time in the range of 0.5−2 ns. It originates, as shown in Figure 1, from a

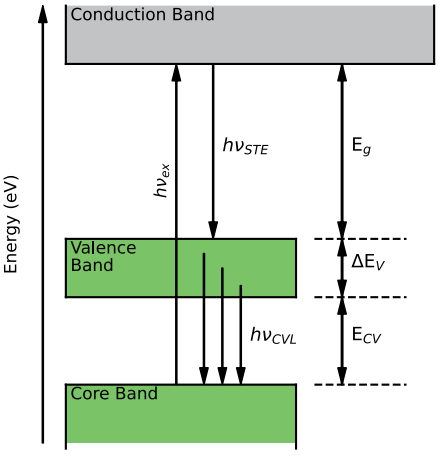

Figure 1. Schematic energy diagram of the electronic bands and transitions involved with bandgap-related luminescence, e.g., self-trapped exciton emission, and CVL, originating from different states of the valence band.

radiative transition between the upper core and the valence band. This transition can occur when an electron is excited from the upper core band to the conduction band, leaving a hole in the upper core band. This hole can recombine with an electron from the valence band, resulting in CVL. This can only occur when

$$(E_{CV} + \Delta E_V) < E_g \quad (1)$$

i.e., the energy difference between the top of the upper core band and the bottom of the valence band (E_{CV}) plus the width of the valence band (ΔE_V) is smaller than the bandgap (E_g). If this condition is not fulfilled, nonradiative Auger processes dominate and CVL will not take place.[26−28] This energy condition is met in some fluoride, chloride, and bromide-based materials containing Ba^{2+}, Cs^+, Rb^+, and K^+ cations.[29]

One of the most well-known scintillators showing CVL is BaF_2 with a decay time of approximately 0.8 ns for its CVL component.[26,30,31] However, BaF_2 also shows a significantly slower decay component, approximately 0.6 μs, originating from self-trapped exciton (STE) emission. Several attempts have been made to suppress this slow STE emission, e.g., by doping BaF_2 with La^{3+}, Y^{3+}, and Sc^{3+}.[32−36] A second challenge for the application of BaF_2 is the short emission wavelength of its CVL emission, i.e., 220, 196, and 183 nm.[28]

Another interesting group of CVL materials are Cs−Cl-based compounds, e.g., CsCl,[37−39] $CsMgCl_3$,[40,41] and $CsCaCl_3$.[42,43] The benefit of Cs−Cl-based compounds over fluoride-based compounds is the shift of the CVL emission to longer wavelengths.[26] Two specific families of Cs−Cl-based compounds, recently gaining attention, are the Cs−Zn−Cl and Cs−Mg−Cl-based compounds.[44,45] The Cs−Zn−Cl family consists of Cs_2ZnCl_4 and Cs_3ZnCl_5, both exclusively showing CVL emission at room temperature. The family of Cs−Mg−Cl compounds consists of $CsMgCl_3$, which is a well-known and studied CVL emitter, Cs_2MgCl_4, and Cs_3MgCl_5. The latter two compounds have only recently been studied for their CVL properties by Rutstrom et al.[45] Similar to the zinc-based compounds, the magnesium-based compounds also mainly show CVL emission at room temperature. It is also possible to tailor the properties of CVL emitters by doping them.[46−50] Rutstrom et al. used this approach to improve the light yield of the Cs−Mg−Cl compounds by doping them with Zn^{2+}.[51] Rutstrom et al.,[52] also substituted part of the Cl^- ions for Br^- ions in Cs_2ZnCl_4, resulting in a further decrease of the decay time. These materials have mainly been studied for their use in time-of-flight positron emission tomography (TOF-PET) and time-of-flight computed tomography (TOF-CT).[44,45,51,53] It should be noted that TOF-CT and photon-counting CT, i.e., a CT system utilizing a PCD instead of an EID, are not the same. An overview of TOF-CT can be found in the work of Rossignol et al.[54]

Unfortunately, very little information is available with regard to the nonproportional response of the Cs−Zn−Cl and Cs−Mg−Cl families of compounds. They have mostly been studied using the 662 keV γ-photons of ^{137}Cs or photons in the UV−vis range. However, most scintillators show a decrease of the light yield upon excitation with lower energy γ-photons or X-rays, e.g., the diagnostic energy range (25−150 keV). This not only affects the signal-to-noise ratio a detector can achieve but may also significantly impact a PCD's ability to discriminate between incident X-ray photons of different energies. Studying the nonproportional response is therefore essential to assess the true potential of these compounds when used in a PCD.

In this work, the two families of Cs−Cl-based compounds, Cs−Zn−Cl and Cs−Mg−Cl, will be studied. The family of Cs−Mg−Cl is studied both with and without 5% Zn^{2+} doping. Additionally, the influence of substituting 5% of the chloride anions with bromide anions on the CVL properties will be studied in Cs_2ZnCl_4. The used doping percentages are based on the optimization study of Rutstrom et al.[51,52] The goal of this work is to assess the suitability of these materials for their

https://doi.org/10.1021/acsaom.5c00253
ACS Appl. Opt. Mater. 2025, 3, 2101−2110

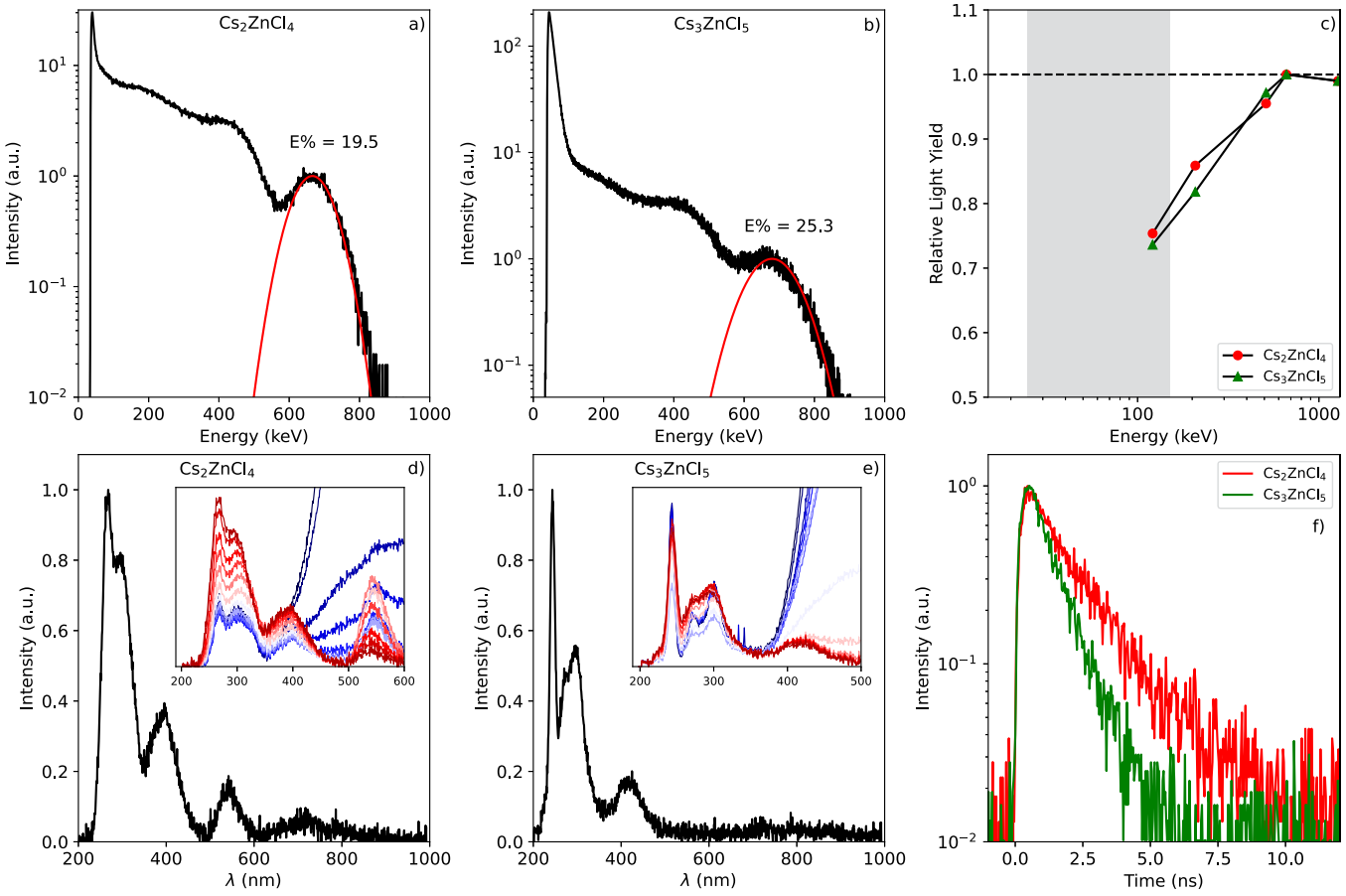

Figure 2. Pulse height spectrum of (a) Cs_2ZnCl_4 and (b) Cs_3ZnCl_5 recorded using the 662 keV γ-photons of ^{137}Cs. (c) Nonproportional response of Cs_2ZnCl_4 and Cs_3ZnCl_5 recorded using the following γ- and X-ray photons: 662 keV of ^{137}Cs, 1275 and 511 keV of ^{22}Na, 208 keV of ^{177}Lu, and 122 keV of ^{57}Co. The ideal response is indicated by the dashed horizontal line at a relative light yield of 1. The gray shaded area indicates the diagnostic energy range (25−150 keV). (d) Room-temperature X-ray-excited emission spectrum of Cs_2ZnCl_4. The inset shows the temperature-dependent behavior of the CVL-related emission bands between 10 and 300 K. (e) Room-temperature X-ray-excited emission spectrum of Cs_3ZnCl_5. The inset shows the temperature-dependent behavior of the CVL-related emission bands between 10 and 300 K. (f) Pulsed X-ray-excited room-temperature decay curves of Cs_2ZnCl_4 and Cs_3ZnCl_5.

use in an indirect PCD. This will be done by studying the not-yet-reported nonproportional response, temperature-dependent X-ray-excited emission spectra, and pulsed X-ray-excited decay curves using X-ray energies in the diagnostic energy range, in order to complement the data published by Rutstrom et al.[44,45,51,52] In addition to the Cs−Zn−Cl and Cs−Mg−Cl compounds, the nonproportional response of BaF_2 will be studied by using a fast digitizer enabling the digitization of individual scintillation pulses. This approach will be used to decompose the nonproportional response of BaF_2 into the contribution of the STE and CVL parts of the emitted scintillation photons.

2. RESULTS AND DISCUSSION

2.1. Scintillation Properties of Cs−Zn−Cl Compounds

Figure 2a,b shows the pulse height spectra of a Cs_2ZnCl_4 and Cs_3ZnCl_5 single crystal (3 mm × 3 mm × 5 mm), respectively. The spectra are measured using a photomultiplier tube (PMT) and 662 keV γ-photons of ^{137}Cs. Based on the full width at half-maximum (fwhm) of the total absorption peak, the energy resolutions of Cs_2ZnCl_4 and Cs_3ZnCl_5 were determined to be 19.5 and 25.3%. The light yields were estimated to be 1,450 and 690 photons/MeV, respectively. The same crystals were used to measure the nonproportional response, utilizing γ-photons of ^{137}Cs, ^{22}Na, ^{177}Lu, and ^{57}Co. The resulting curves of both compounds are shown in Figure 2c. The ideal nonproportionality response is represented by the dashed horizontal line at a relative light yield of 1. The gray marked area indicates the diagnostic energy range (25−150 keV), the operation range of an indirect PCD. Between 662 and 122 keV, both compounds show a strong drop in their nonproportional response. The curves could not be extended below 122 keV due to the small photon yields at these deposition energies, resulting in a large uncertainty in the relative light yield. A strong decrease of the light yield is typically not observed in the nonproportional response of Ce^{3+}-doped halide scintillators.[55−57] It is more commonly observed in Ce^{3+}- or Pr^{3+}-activated oxide-based scintillators, but not to the same degree as observed for CVL in Cs_2ZnCl_4 and Cs_3ZnCl_5.[55−57] The drop in the nonproportional response within the diagnostic energy range will significantly deteriorate the energy resolution of both Cs_2ZnCl_4 and Cs_3ZnCl_5 at these deposition energies. Hence, it is difficult for a PCD based on these materials to discriminate the energy of incident X-ray photons.

The room-temperature X-ray-excited emission spectrum of Cs_2ZnCl_4, shown in Figure 2d, contains four emission bands

https://doi.org/10.1021/acsaom.5c00253
ACS Appl. Opt. Mater. 2025, 3, 2101−2110

Table 1. Overview of Scintillation Properties of the Studied Cs−Zn−Cl and Cs−Mg−Cl Compounds[a]

	LY at 662 keV (Ph/MeV)	E % at 662 keV	τ_{dec} (ns)	$\lambda_{em,peak}$ (nm)		ρ (g/cm^3)
Cs_2ZnCl_4	1450	19.5	1.76	265	300	3.35
				395	540	
Cs_3ZnCl_5	690	25.3	0.99	245	295	3.44
				415		
$Cs_2ZnCl_{3.8}Br_{0.2}$	670	24	1.43	265	300	3.35
				395	520	
$CsMgCl_3$	1800	20.4	2.2	280	480	3.23
$CsMgCl_3$:Zn^{2+}	2450	14.1	2.08	280	420	3.23
				650		
Cs_2MgCl_4	1900	17.6	1.98	275	315	2.95
				400		
Cs_2MgCl_4:Zn^{2+}	2000	18	1.95	275	410	2.95
Cs_3MgCl_5	760	23.5	1.64	240	300	3.15
Cs_3MgCl_5:Zn^{2+}	1200	19.6	1.54	240	300	3.15

[a]The tabulated properties are the light yield at 662 keV (LY (Ph/MeV)), energy resolution measured at 662 keV (E %), pulsed X-ray-excited decay time (τ_{dec} (ns)), X-ray-excited peak emission wavelengths ($\lambda_{em,peak}$ (nm)), and mass density (ρ (g/cm^3)).

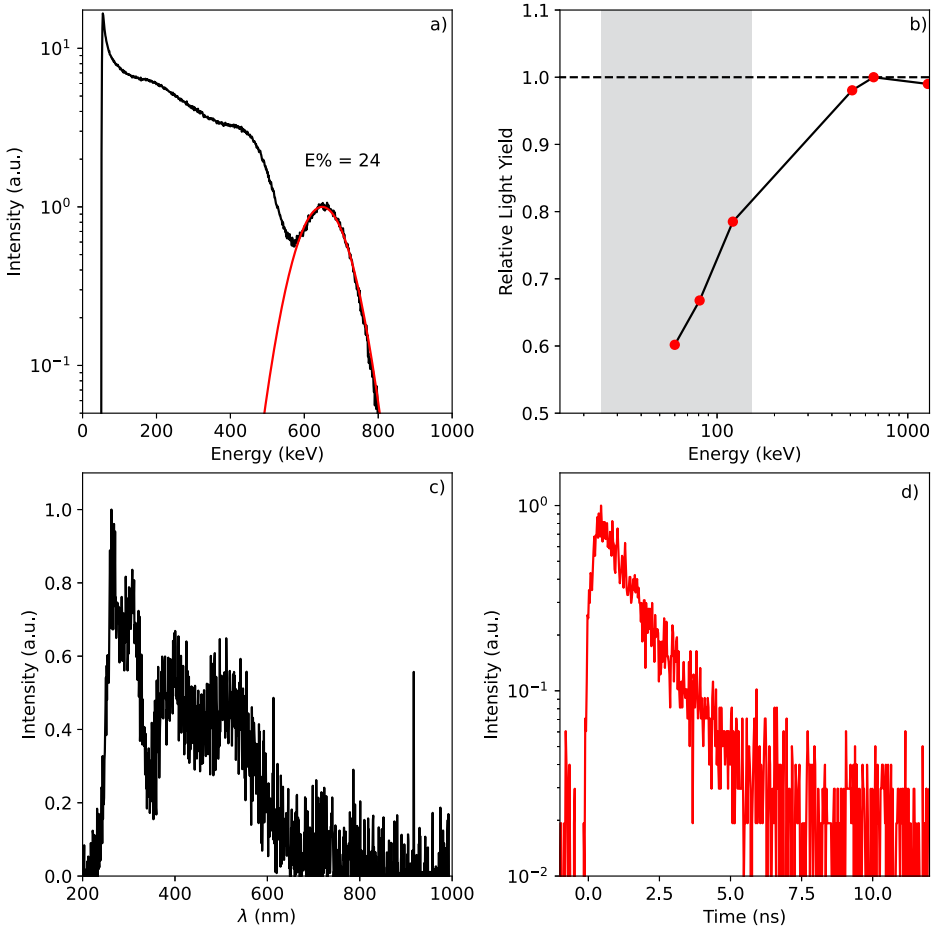

Figure 3. (a) Pulse height spectrum of $Cs_2ZnCl_{3.8}Br_{0.2}$ recorded using the 662 keV γ-photons of ^{137}Cs. (b) Nonproportional response of $Cs_2ZnCl_{3.8}Br_{0.2}$ recorded using the following γ- and X-ray photons: 662 keV of ^{137}Cs, 1275 and 511 keV of ^{22}Na, 122 keV of ^{57}Co, 81 keV of ^{133}Ba, and 60 keV of ^{241}Am. The ideal response is indicated by the dashed horizontal line, at a relative light yield of 1. The gray shaded area indicates the diagnostic energy range (25−150 keV). (c) Room-temperature X-ray-excited emission spectrum of $Cs_2ZnCl_{3.8}Br_{0.2}$. (d) Pulsed X-ray-excited room-temperature decay curve of $Cs_2ZnCl_{3.8}Br_{0.2}$.

located at 265 nm (4.68 eV), 300 nm (4.13 eV), 395 nm (3.14 eV), and 540 nm (2.30 eV). The 265, 300, and 395 nm emission bands have also been observed by Rutstrom et al.,[44] Yahaba et al.,[58] and Takahashi et al.,[59] all assigning the bands to CVL. The less-intense 540 nm emission band has also been observed by Ohnishi et al.,[60] who suggested it to be related to lattice defects. The inset in Figure 2d shows the temperature-dependent behavior of the CVL bands between 10 and 325 K. The temperature dependence of the complete X-ray-excited emission spectrum and integrated emission intensities can be

https://doi.org/10.1021/acsaom.5c00253
ACS Appl. Opt. Mater. 2025, 3, 2101−2110

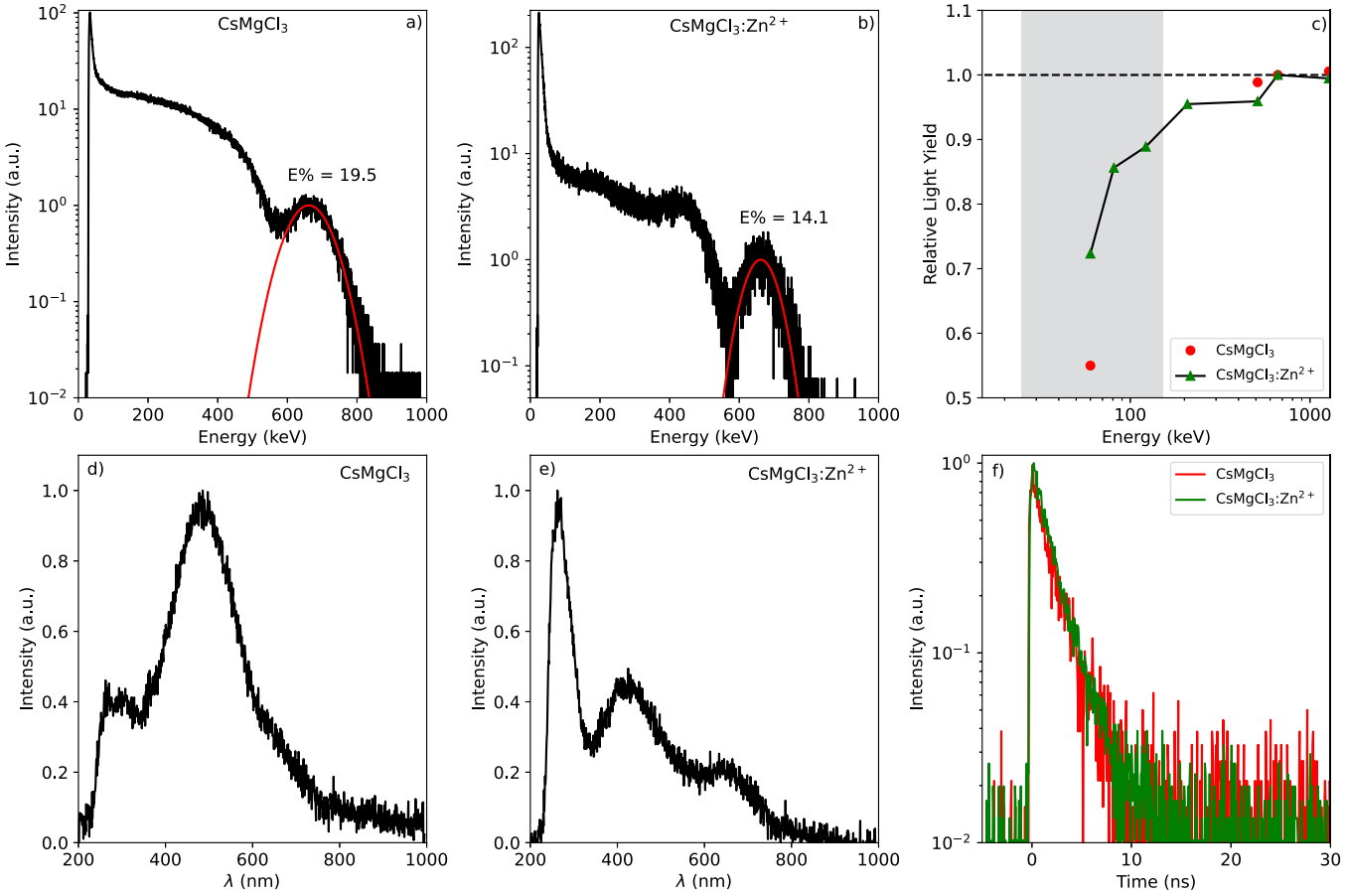

Figure 4. Pulse height spectrum of (a) $CsMgCl_3$ and (b) $CsMgCl_3$: 5% Zn^{2+} recorded using the 662 keV γ-photons of ^{137}Cs. (c) Nonproportional response of $CsMgCl_3$ and $CsMgCl_3$: 5% Zn^{2+} recorded using the following γ- and X-ray photons: 662 keV of ^{137}Cs, 1275 and 511 keV of ^{22}Na, 122 keV of ^{57}Co, 81 keV of ^{133}Ba, and 60 keV of ^{241}Am. The ideal response is indicated by the dashed horizontal line, at a relative light yield of 1. The gray shaded area indicates the diagnostic energy range (25−150 keV). (d) Room-temperature X-ray-excited emission spectrum of $CsMgCl_3$. (e) Room-temperature X-ray-excited emission spectrum of $CsMgCl_3$: 5% Zn^{2+}. (f) Pulsed X-ray-excited room-temperature decay curves of $CsMgCl_3$ and $CsMgCl_3$: 5% Zn^{2+}.

found in Figure S1. At 10 K, two additional emission bands are observed at 520 and 670 nm, which have not been observed before and quench completely above 100 K. In contrast, the intensity of the CVL bands increases upon going from 10 to 325 K. This behavior has also been observed in other CVL emitters, e.g., BaF_2.[27,61,62]

The room-temperature X-ray-excited emission spectrum of Cs_3ZnCl_5, shown in Figure 2e, contains three emission bands located at 245 (5.06 eV), 295 (4.20 eV), and 415 nm (2.99 eV). These emission bands have also been observed by Rutstrom et al.[44] and Takahashi et al.,[59] ascribing all bands to CVL. The inset in Figure 2e shows the temperature-dependent behavior of the CVL bands between 10 and 325 K. The temperature dependence of the complete X-ray-excited emission spectrum and integrated emission intensities can be found in Figure S1. At 10 K, two additional emission bands are observed at 520 and 900 nm, which have not been observed before, and quench completely above 200 K. Similar to Cs_2ZnCl_4, the integrated CVL emission intensities of Cs_3ZnCl_5 also show an increase in intensity upon heating from 10 to 325 K.

The room-temperature pulsed X-ray-excited decay curves, using X-rays with an average energy of 18.2 keV, of Cs_2ZnCl_4 and Cs_3ZnCl_5 are shown in Figure 2f. Both decay curves show one decay component; hence, a single exponential model is used to determine the decay times. The decay times of Cs_2ZnCl_4 and Cs_3ZnCl_5 were determined to be 1.76 and 0.99 ns, respectively. Similar values have been observed by Rutstrom et al., using the 662 keV γ-photons of ^{137}Cs, and Takahashi et al.[59] under optical excitation. However, Takahashi et al. also observed an additional decay component for both Cs_2ZnCl_4 and Cs_3ZnCl_5 of approximately 15 ns. These were not observed in the decay curves shown in Figure 2f. The scintillation properties of Cs_2ZnCl_4 and Cs_3ZnCl_5 are summarized in Table 1.

2.2. Influence of Br^- Doping on Cs_2ZnCl_4

One of the potential ways of tailoring the scintillation properties of the Cs−Cl-based CVL emitters is by replacing part of the chloride anions with bromide anions. Figure 3a shows the pulse height spectrum of a $Cs_2ZnCl_{3.8}Br_{0.2}$ single crystal (3 mm × 3 mm × 5 mm) recorded using the 662 keV γ-photons of ^{137}Cs. Based on the fwhm of the total absorption peak, the energy resolution of $Cs_2ZnCl_{3.8}Br_{0.2}$ was determined to be 24%. The light yield was determined to be 670 photons/MeV, which is approximately half that of undoped Cs_2ZnCl_4. The same crystal was used to measure the nonproportional response of $Cs_2ZnCl_{3.8}Br_{0.2}$, utilizing γ-photons of ^{137}Cs, ^{22}Na, ^{57}Co, ^{133}Ba, and ^{241}Am. Again, the ideal nonproportionality response is represented by the horizontal dashed line and the

https://doi.org/10.1021/acsaom.5c00253
ACS Appl. Opt. Mater. 2025, 3, 2101−2110

diagnostic energy range (25−150 keV) by the gray marked area. The nonproportional response of $Cs_2ZnCl_{3.8}Br_{0.2}$ shows a drop of 40% between 662 and 60 keV. The curve could not be extended beyond 60 keV due to the diminishing photon yield at lower deposition energies. Similar to the undoped Cs−Zn−Cl compounds, the drop of the nonproportional response within the diagnostic energy range will make it difficult for a PCD based on $Cs_2ZnCl_{3.8}Br_{0.2}$ to discriminate the energies of incident X-ray photons.

The room-temperature X-ray-excited emission spectrum of $Cs_2ZnCl_{3.8}Br_{0.2}$ is shown in Figure 3c. The spectrum contains four emission bands located at 265 nm (4.68 ev), 300 nm (4.13 eV), 395 nm (3.14 eV), and 520 nm (2.38 eV). This is very similar to the emission bands observed for Cs_2ZnCl_4, as shown in Figure 2d. The temperature dependence of the X-ray-excited emission spectrum and integrated emission intensities between 10 and 325 K can be found in Figure S2. The room-temperature pulsed X-ray-excited decay curve of $Cs_2ZnCl_{3.8}Br_{0.2}$ is shown in Figure 3d. Similar to the decay curve of Cs_2ZnCl_4, shown in Figure 2f, only one decay component is observed. The decay time of $Cs_2ZnCl_{3.8}Br_{0.2}$ was determined to be 1.43 ns, which is 330 ps faster compared to the decay time of Cs_2ZnCl_4. The scintillation properties of $Cs_2ZnCl_{3.8}Br_{0.2}$ are summarized in Table 1.

2.3. Scintillation Properties of Cs−Mg−Cl Compounds and the Role of Zn^{2+} Doping

The second group of studied compounds is the compounds in the Cs−Mg−Cl family, for which each member is studied with and without 5% Zn^{2+} doping. Figure 4a,b shows the pulse height spectra of $CsMgCl_3$ and $CsMgCl_3$:Zn^{2+} single crystals (3 mm × 3 mm × 5 mm), respectively. The spectra are recorded using a PMT and 662 keV γ-photons of ^{137}Cs. Based on the fwhm of the total absorption peak, the energy resolutions of $CsMgCl_3$ and $CsMgCl_3$:Zn^{2+} were determined to be 19.5 and 14.1%, and the light yields were 1800 and 2,450 photons/MeV, respectively. The increase of the light yield upon Zn^{2+} doping was observed by Rutstrom et al.[51] The same crystals were used to determine the nonproportional response of these compounds utilizing γ photons of ^{137}Cs, ^{22}Na, ^{57}Co, ^{133}Ba, and ^{241}Am. The resulting curve is shown in Figure 4c. Again, the ideal nonproportionality response is represented by the horizontal dashed line and the diagnostic energy range (25−150 keV) by the gray marked area. Similar to the Cs−Zn−Cl compounds, the $CsMgCl_3$ compounds also showed a strong drop in their light yield. The light yield of $CsMgCl_3$ decreases by 40% between 662 and 60 keV. Doping $CsMgCl_3$ seems to improve the nonproportional response, showing a decrease of 30% between 662 and 60 keV. Similar to the Cs−Zn−Cl compounds, the nonproportional response could not be extended to deposition energies below 60 keV due to diminishing photon yields.

The room-temperature X-ray-excited emission spectrum of $CsMgCl_3$ is shown in Figure 4d. The spectrum contains two emission bands located at 280 nm (4.43 eV) and 480 nm (2.58 eV); the latter also shows a shoulder on the long wavelength side. These bands have also been observed by Rutstrom et al.[51] and Vanecek et al.[43] The latter assigns the 280 nm emission band to CVL and the 480 nm emission band to a bandgap-related emission process, i.e., STE or defect-related emission. The temperature dependence of the X-ray-excited emission spectra and integrated emission intensities of $CsMgCl_3$ can be found in Figure S3. Upon cooling down, the intensity of the 480 nm emission band increases, showing the classical quenching behavior expected of STE emission.

The room-temperature X-ray-excited emission spectrum of $CsMgCl_3$:Zn^{2+} is shown in Figure 4e. The spectrum contains three emission bands located at 280 nm (4.43 eV), 480 nm (2.58 eV), and 650 nm (1.91 eV). These are the same bands as those observed in the emission spectrum of the undoped $CsMgCl_3$, shown in Figure 4d. The most important difference is the suppression of the 480 nm emission band by the Zn^{2+} doping, revealing the 680 nm emission peak, which is observed as a shoulder in the spectrum of the undoped $CsMgCl_3$. The temperature-dependent behavior of the X-ray-excited emission spectra and integrated emission intensities of $CsMgCl_3$:Zn^{2+} can be found in Figure S3.

The room-temperature pulsed X-ray-excited decay curves of $CsMgCl_3$ and $CsMgCl_3$:Zn^{2+} are shown in Figure 4f. The decay curves for both compounds look very similar and show only one decay component. The decay times of $CsMgCl_3$ and $CsMgCl_3$:Zn^{2+} were determined to be 2.2 and 2.08 ns, respectively. Similar decay times have been observed by Rutstrom et al.[51] and Vanecek et al.[43] The latter also observed a very weak, below 1% intensity, decay component under γ-photon excitation. This decay component was not observed in our measurement. The scintillation properties of $CsMgCl_3$ and $CsMgCl_3$:Zn^{2+} are summarized in Table 1.

The characterization of Cs_2MgCl_4 and Cs_2MgCl_4:Zn^{2+} is shown in Figure S4. The light yield, energy resolution, emission wavelengths, and decay times of both compounds are summarized in Table 1. Both compounds, similar to the doped and undoped $CsMgCl_3$, show a strong drop in their nonproportional response below 662 keV. The X-ray-excited emission spectra of both compounds are similar to the ones published by Rutstrom et al.[45,51] The temperature-dependent X-ray-excited emission spectra and integrated emission intensities of both compounds are shown in Figure S5. One interesting feature is that the additional emission band observed for Cs_2MgCl_4 below 150 K is no longer observed for Cs_2MgCl_4:Zn^{2+}.

The characterization of Cs_3MgCl_5 and Cs_3MgCl_5:Zn^{2+} is shown in Figure S6. The light yield, energy resolution, emission wavelengths, and decay times of both compounds are summarized in Table 1. Similar to the other members of the Cs−Mg−Cl family of compounds, the nonproportionality of Cs_3MgCl_5 and Cs_3MgCl_5:Zn^{2+} shows a significant drop of 40 and 80% between 662 and 60 keV, respectively. The X-ray-excited emission spectra of both compounds are similar to those published by Rutstrom et al.[45,51] The temperature-dependent X-ray-excited emission spectra and integrated emission intensities of both compounds are shown in Figure S7.

2.4. Decomposing the Nonproportional Response of BaF_2

The nonproportional response of BaF_2, in comparison to those measured for the Cs−Zn−Cl and Cs−Mg−Cl shown in Figure 2c, 3b, and 4c, does not show a strong drop.[55] However, the majority of the scintillation photons emitted by BaF_2 originate from STE emission, and approximately 15% originate from the CVL component.[26] The contribution of the STE luminescence and CVL to the nonproportional response of BaF_2 can, however, be separated by utilizing fast digitization of individual scintillation pulses. A similar approach was used by Wolszczak and Dorenbos to study the pulse shape change as a function of

https://doi.org/10.1021/acsaom.5c00253
ACS Appl. Opt. Mater. 2025, 3, 2101−2110

deposition energy in CsI:Tl$^+$.[63] In this work, we will refer to this approach as pulse shape decomposition analysis (PSDA).

The PSDA starts by digitizing a large set (1000+) of scintillation pulses generated by a radioactive source in BaF_2. The first step in the analysis is to remove pulses consisting of pile-up events from the measured set. Each pulse in the set will contain a fast decay component from the CVL and a slow decay component from the STE luminescence. The goal is to determine the ratio between these components as a function of the deposited gamma or X-ray energy in the scintillator. The integrated intensity of the filtered scintillation pulses is then used to reconstruct a pulse height spectrum. Only those pulses that correspond to energy bins within the total absorption peak are used for further analysis. The selected scintillation pulses are used to establish the average pulse shape corresponding to the deposition energy of the total absorption peak of the used source. The average pulse shapes are fitted using two exponential decay curves in order to determine the contribution of the STE and CVL components to the total intensity of the scintillation pulse at the specified deposition energy. This approach allows us to determine the change of the CVL contribution to the total signal as a function of deposition energy and hence to decompose the nonproportional response of BaF_2.

The resulting curves of PSDA are shown in Figure 5. The PSDA shows that the nonproportional response of the CVL

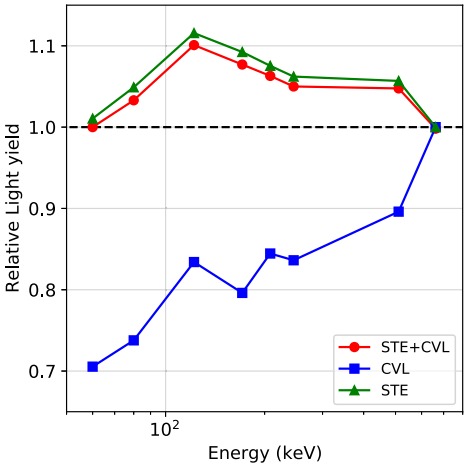

Figure 5. Nonproportionality response and decomposed non-proportionality response of BaF_2. The ideal response is indicated by the dashed horizontal line, at a relative light yield of 1. The pulse shapes used for the decomposition were obtained using 662 keV (^{137}Cs), 511 keV (^{22}Na), 245 and 171 keV (^{111}In), 208 keV (^{177}Lu), 122 keV (^{57}Co), 81 keV (^{133}Ba), and 60 keV (^{241}Am) γ-photons.

emission of BaF_2 shows a similar drop at lower deposition energies as observed for the Cs−Zn−Cl and Cs−Mg−Cl compounds. The nonproportional response of the CVL component decreases by 30% between 662 and 60 keV. This decrease in deposition energy corresponds to an increase of the ionization density, which is known to influence the CVL intensity.[28] For example, it has been shown that BaF_2 shows no CVL emission under α particle excitation, which creates short ionization tracks with a very high ionization density.[64,65] Similar behavior is also observed in Cs−Cl-based compounds like CsCl[66] and compounds like $Cs_2LiLaCl_6$[67] and Cs_2LiYCl_6[68] where the absence of CVL under alpha excitation and the presence under gamma excitation are used for pulse shape discrimination. For both BaF_2 and CsCl, it has also been demonstrated in cathodoluminescence studies that the CVL intensity decreased upon decreasing the acceleration voltage, which corresponds to decreasing the kinetic energy of the electrons used for excitation and thus an increase of the ionization density.[69] To the best of our knowledge, evidence of the decrease of the CVL intensity under γ-photon excitation in BaF_2 has never been shown.

3. CONCLUSIONS

In this work, two families of Cs−Cl-based compounds, Cs−Zn−Cl and Cs−Mg−Cl, have been studied for their potential application in an indirect PCD. All compounds show single exponential decay behavior, with lifetimes in the range of 0.99−2.2 ns, making these materials suitable to handle the high X-ray incident fluence rates of an imaging task. However, the nonproportional response of all compounds shows a strong decrease of the light yield in the diagnostic energy range (25−150 keV). This significantly deteriorates the energy resolution attainable with these materials in the operation range of an indirect PCD (25−150 keV), i.e., they will not be able to efficiently discriminate the energies of incident X-ray photons. The nonproportional response of the CVL component of BaF_2 was also studied by utilizing the fast digitization of individual scintillation pulses. It was shown that the nonproportional response of the CVL component of BaF_2 also shows a strong decrease in the diagnostic energy range, which is normally not observable due to the presence of STE emission. This, in addition to the short emission wavelength of the CVL component of BaF_2 and the presence of the slower STE emission, forms a third reason why BaF_2 is not suitable to be used in an indirect PCD.

4. EXPERIMENTAL SECTION

The crystals used in this work were grown at the University of Tennessee. Information on the synthesis of the Cs−Zn−Cl crystals can be found in ref 44. Information on the synthesis of Cs_2MgCl_4 and Cs_3MgCl_5 can be found in ref 45. Information on the synthesis of $CsMgCl_3$ and the Zn^{2+} doped Cs−Mg−Cl compounds can be found in ref 51. Information on the synthesis of $Cs_2ZnCl_{3.8}Br_{0.2}$ can be found in ref 52. Information on the powder X-ray diffraction and pictures of the crystals can be found in the respective references cited above.

Pulse height spectra were recorded using a Hamamatsu Super Bialkali R6231-100 (SN ZE4500) PMT, operated at −700 V. The samples were mounted using optical coupling and covered with PTFE tape. The signal was processed by an integrated preamplifier and an Ortec 672 spectroscopic amplifier. The signal was digitized by an Ortec AD144 26 K ADC. All spectra were recorded using a shaping time of 0.5 μs. Light yields were determined according to the method described by de Haas and Dorenbos.[70] The nonproportionality curves were recorded using the same PMT using γ-photons of ^{137}Cs, ^{22}Na, ^{177}Lu, ^{57}Co, ^{133}Ba, and ^{241}Am.

The presented X-ray-excited emission spectra were recorded using X-rays from a tungsten anode X-ray tube, operated at 79 kV. This produces X-ray photons with an average energy of 40 keV. The low energy side of the created X-ray spectrum was removed by placing a 3 mm aluminum filter between the X-ray tube and the sample in order to prevent radiation damage. Temperature-dependent measurements were performed by mounting the samples on a closed-cycle helium cryostat. The emitted light was detected by an Ocean Insights QE pro photospectrometer.

The presented pulsed X-ray-excited decay curves were recorded using the time-correlated single-photon method. The X-ray pulse was generated by a Hamamatsu N5084 light excited X-ray tube, excited by a PicoQuant LDH−P-C-440 M pulsed diode laser, producing X-ray pulses with an average energy of 18.2 keV. The reference output of

https://doi.org/10.1021/acsaom.5c00253
ACS Appl. Opt. Mater. 2025, 3, 2101−2110

the PicoQuant laser driver was used as the start signal and was connected to an Ortec 567 time-to-amplitude converter (TAC). The emitted photons were detected by an ID Quantique id100-50 single-photon counter, generating a stop signal. The output signal of the TAC was digitized by an Ortec AD 114 ADC.

The deconvolution of the nonproportional response of BaF_2 using pulse shape discrimination was performed by mounting a BaF_2 crystal on a Philips XP20Q PMT using optical coupling. The crystal was covered with a PTFE tape. The separate scintillation pulses were processed and digitized by a CAEN DT5761 desktop digitizer. The scintillation pulses were recorded using γ-photons of ^{137}Cs, ^{22}Na, ^{111}In, ^{177}Lu, ^{57}Co, ^{133}Ba, and ^{241}Am.

■ ASSOCIATED CONTENT

Supporting Information

The Supporting Information is available free of charge at https://pubs.acs.org/doi/10.1021/acsaom.5c00253.

Temperature-dependent X-ray-excited emission spectra of all compounds, pulse height spectra, nonproportional response, room-temperature X-ray-excited emission spectra, and pulsed X-ray-excited decay curves of Cs_2MgCl_4 and Cs_3MgCl_5 with and without Zn^{2+} (PDF)

■ AUTHOR INFORMATION

Corresponding Authors

J. Jasper van Blaaderen − *Faculty of Applied Sciences, Department of Radiation Science and Technology, Delft University of Technology, 2629 JB Delft, Netherlands;* orcid.org/0000-0003-1460-8319; Email: J.J.vanBlaaderen@tudelft.nl

Pieter Dorenbos − *Faculty of Applied Sciences, Department of Radiation Science and Technology, Delft University of Technology, 2629 JB Delft, Netherlands;* Email: P.Dorenbos@tudelft.nl

Authors

Daniel Rutstrom − *Scintillation Materials Research Centre, University of Tennessee Knoxville, Knoxville, Tennessee 37996, United States; Department of Materials Science and Engineering, University of Tennessee Knoxville, Knoxville, Tennessee 37996, United States*

Giles Bangoyina − *Faculty of Applied Sciences, Department of Radiation Science and Technology, Delft University of Technology, 2629 JB Delft, Netherlands*

Luis Stand − *Scintillation Materials Research Centre, University of Tennessee Knoxville, Knoxville, Tennessee 37996, United States; Department of Nuclear Engineering, University of Tennessee Knoxville, Knoxville, Tennessee 37996, United States;* orcid.org/0000-0001-6846-8986

Casper van Aarle − *Faculty of Applied Sciences, Department of Radiation Science and Technology, Delft University of Technology, 2629 JB Delft, Netherlands*

Johan de Haas − *Faculty of Applied Sciences, Department of Radiation Science and Technology, Delft University of Technology, 2629 JB Delft, Netherlands*

Dennis R. Schaart − *Faculty of Applied Sciences, Department of Radiation Science and Technology, Delft University of Technology, 2629 JB Delft, Netherlands; Holland Proton Therapy Center, 2629 JH Delft, Netherlands*

Charles L. Melcher − *Scintillation Materials Research Centre, University of Tennessee Knoxville, Knoxville, Tennessee 37996, United States; Department of Materials Science and Engineering and Department of Nuclear Engineering, University of Tennessee Knoxville, Knoxville, Tennessee 37996, United States*

Mariya Zhuravleva − *Scintillation Materials Research Centre, University of Tennessee Knoxville, Knoxville, Tennessee 37996, United States; Department of Materials Science and Engineering, University of Tennessee Knoxville, Knoxville, Tennessee 37996, United States*

Complete contact information is available at: https://pubs.acs.org/10.1021/acsaom.5c00253

Notes

The authors declare no competing financial interest.

■ ACKNOWLEDGMENTS

The authors would like to thank Robin De Kruijff, Astrid van der Meer, and Folkert Geuring for their support in obtaining the different sources used in this work. J.J.v.B. would also like to thank Anthony Burch, Freddie Wong, Matt Arnold, Will Campos, and Beth May for all of the fruitful discussions. The authors acknowledge financial support from TTW/OTP grant no. 18040 and the support from the Department of Energy National Nuclear Security Administration through the Nuclear Science and Security Consortium under Award Number DE-NA-0003996.

■ REFERENCES

(1) Flohr, T.; Petersilka, M.; Henning, A.; Ulzheimer, S.; Ferda, J.; Schmidt, B. Photon-Counting CT review. *European Journal of Medical Physics* **2020**, *79*, 126−136.

(2) Hsieh, S. S.; Leng, S.; Rajendran, K.; Tao, S.; McCollough, C. H. Photon Counting CT: Clinical Applications and Future Developments. *IEEE Transactions on Radiation and Plasma Medical Sciences* **2021**, *5* (4), 441−452.

(3) Taguchi, K.; Iwanczyk, J. S. Vision 20/20: Single photon counting X-ray detectors in medical imaging. *Med. Phys.* **2013**, *40* (10), 100901.

(4) Flohr, T.; Ulzheimer, S.; Petersilka, M.; Schmidt, B. Basic principles and clinical potential of photon-counting detector CT. *Chinese Journal of Academic Radiology* **2020**, *3*, 19−34.

(5) Benson, J. C.; Rajendran, K.; Lane, J. I.; Diehn, F. E.; Weber, N. M.; Thorne, J. E.; Larson, N. B.; Fletcher, J. G.; McCollough, C. H.; Leng, S. *Americal Journal of Neuroradiology* **2022**, *43* (4), 579−584.

(6) Hagen, F.; Soschynski, M.; Weis, M.; Hagar, M. T.; Krumm, P.; Ayx, I.; Taron, J.; Krauss, T.; Hein, M.; Ruile, P.; Meuhlen, v. z.; Schlett, C. L.; Neubauer, J.; Tsiflikas, I.; Russe, M. F.; Arnold, P.; Faby, S.; Froelich, M. F.; Weiss, J.; Stein, T.; Overhoff, D.; Bongers, M.; Nikolaou, K.; Schonberg, S. O.; Bamberg, F.; Horger, M. Photon-counting computed tomography - clinical application in oncological, cardiovascular, and pediatric radiology. *Rofo* **2024**, *196* (1), 25−35.

(7) Kappler, S.; Henning, A.; Kreisler, B.; Schoeck, F.; Stierstorfer, K.; Flohr, T. Photon counting CT at elevated X-ray tube current: Contrast stability, image noise and multi - energy performance. In *Proceedings Volume 9033, Medical Imaging 2014: Physics of medical imaging, 90331C*, 2014.

(8) Steadman, R.; Herrmann, C.; Livne, A. ChromAIX2: A large area, high count-rate energy-resolving photon counting ASIC for a spectral CT prototype. *Nuclear Instruments and Methods in Physics Research Section A: Accelerators, Spectrometers, Detectors and Associated Equipment* **2017**, *862*, 18−24.

(9) da Silva, J.; Gronberg, F.; Cederstrom, B.; Persson, M.; Sjolin, M.; Alagic, Z.; Bujila, R.; Danielsson, M. Resolution characterization of a silicon-based. photon-counting computed tomography prototype capable of patient scanning. *J. Med. Imaging* **2019**, *6* (4), No. 043502.

(10) Sundberg, C.; Danielsson, M.; Persson, M. U. Compton coincidence in silicon photon-vounting CT detectors. *Journal of Medical Imaing* **2022**, *9* (1), No. 013501.
(11) Danielsson, M.; Persson, M.; Sjolin, M. Photon counting X-ray detectors for CT. *Phys. Med. Biol.* **2021**, *66*, No. 03TR01.
(12) Taguchi, K.; Schaart, D. R.; Goorden, M. C.; Hsieh, S. S. Imaging performance of a $LaBr_3$:Ce scintillation detector for photon counting X-ray computed tomography: Simulation study. *International Journal of Medical Physics Research and Practice* **2025**, *52*, 158.
(13) Bizarri, G.; Dorenbos, P. Charge carrier and exciton dynamics in $LaBr_3$:Ce^{3+} scintillators: Experiment and model. *Phys. Rev. B* **2007**, *75*, No. 184302.
(14) van der Sar, S. J. Exploring X-ray photon-counting scintillation detectors with silicon photomultiplier readout for medical imaging, 2023.
(15) van der Sar, S. J.; Brunner, S. E.; Schaart, D. R. Silicon photomultiplier-based scintillation detectors for photon-counting CT: A feasibility study. *Med. Phys.* **2021**, *48*, 6324−6338.
(16) van der Sar, S. J.; Leibold, D.; Brunner, S. E.; Schaart, D. R. LaBr3:Ce and silicon photomultipliers: towards optimal scintillating photon-counting detector. In *Proceedings Volume 12304, 7th International conference on Image Formation in X-ray Computed Tomography, 12304A*, 2022.
(17) van der Sar, S. J.; Brunner, S.; Schaart, D. X-ray photon-counting using silicon photomultiplier-based scintillation detectors at high X-ray tube currents. In *Proceedings Volume 12031, Medical Imaging 2022: Physics of Medical Imaging, 1203101*, 2022.
(18) Arimoto, M.; Morita, H.; Fujieda, K.; Maruhashi, T.; Kataoka, J.; Nitta, H.; Ikeda, H. Development of LSI for a new kind of photon-counting computed tomography using multipixel photon counters. *Nucl. Instrum. Methods Phys. Res., Sect. A* **2018**, *912*, 186.
(19) Kiji, H.; Maruhashi, T.; Toyoda, T.; Kataoka, J.; Arimoto, M.; Sato, D.; Yoshiura, K.; Kabayashi, S.; Kawashima, H.; Terazawa, S.; Shiota, S.; Ikeda, H. 64-Channel photon-counting computed tomography using a new MPPC-CT system. *Nucl. Instrum. Methods Phys. Res., Sect. A* **2020**, *984*, No. 164610.
(20) Maruhashi, T.; Morita, H.; Arimoto, M.; Kataoka, J.; Fujieda, K.; Nitta, H.; Ikeda, H.; Kiji, H. Evaluation of a novel photon-counting CT system using a 16-channel MPPC array for multicolor 3-D imaging. *Nucl. Instrum. Methods Phys. Res., Sect. A* **2019**, *936*, 5.
(21) Sato, D.; Arimoto, M.; Ishiguro, A.; Lucyana, F.; Tomoda, T.; Okumura, K.; Kawashima, H.; Kobayashi, S.; Murakami, K.; Kataoka, J.; Sagisaka, M.; Terazawa, S.; Shiota, S. Multi-energy in-vivo imaging of multiple contrast agents in a mouse using MPPC-based photon-counting CT, Nuclear Instruments and Methods in Physics Reserach Section A: Accelerators, Spectromoeters. *Detectors and Associated Equipment* **2024**, *1064*, No. 169337.
(22) Shimazoe, K.; Kim, D.; Hamdan, M.; Kamada, K.; Yoshino, M.; Shoji, Y.; Sakamoto, K.; Acerbi, F.; Gola, A. Scintillator-single-photon avalanche diode array-based energy resolving photon counting X-ray detector, preprint, 2024.
(23) van Blaaderen, J. J.; van der Sar, S.; Onggo, D.; Sheikh, Md. A. K.; Schaart, D. R.; Birowosuto, M. D.; Dorenbos, P. $(BZA)_2PbBr_4$: A potential scintillator for photon-counting computed tomography detectors. *J. Lumin.* **2023**, *263*, No. 120012.
(24) van Blaaderen, J. J.; van Aarle, C.; Leibold; Dorenbos, P.; Schaart, D. R. Guidelines for the Selection of Scintillators for Indirect Photon-Counting X-ray Detectors. *Chem. Mater.* **2025**, *37* (5), 1716−1740.
(25) van Eijk, C. W. E. Cross-luminescence. *J. Lumin.* **1994**, *60*−*61*, 936−941.
(26) Khanin, V.; Venevtsev, I.; Rodnyi, P. Recent advances in the study of core-valence luminescence (cross luminescence). *Review, Optical Materials* **2023**, *136*, No. 113399.
(27) Itoh, M.; Kamada, M.; Ohno, N. Temperature dependence of auger-free luminescence in alkali and alkaline-earth halides. *J. Phys. Soc. Jpn.* **1997**, *66*, 2502−2512.
(28) Rodnyi, P. A. Core-valence luminescence in scintillators. *Radiat. Meas.* **2004**, *38* (4−6), 343−352.
(29) Rodnyi, P. A. Choice of compounds with fast core-valence transitions. *MRS Online Proc. Libr.* **1994**, *348*, 77−88.
(30) Laval, M.; Moszynski, M.; Allemand, R.; Cormoreche, E.; Guinet, P.; Odru, R.; Vacher, J. Barium fluoride - Inogranic scintillator for subnanosecond timing. *Nucl. Instrum. Methods Phys. Res.* **1983**, *206* (1−2), 169−176.
(31) Lewellen, T. K. Time-of-flight PET. *Seminars in Nuclear Medicine* **1998**, *28* (3), 268−275.
(32) Dorenbos, P.; Visser, R.; Dool, R.; Andriessen, J.; van Eijk, C. W. E. Suppression of self-trapped exciton luminescence in La^{3+}- and Nd^{3+}- doped BaF_2. *J. Phys.: Condens. Matter* **1992**, *4* (23), 5281.
(33) Radzhabov, E.; Istomin, A.; Nepomnyashik, A.; Egranov, A.; Ivasheckin, V. Excitonic interaction with impurity in barium fluoride crystals. *Nucl. Instrum. Methods Phys. Res., Sect. A* **2005**, *537* (1−2), 71−75.
(34) Gundacker, S.; Pots, R. H.; Nepomnyashchikh, A.; Radzhabov, E.; Shendrik, R.; Omelkov, S.; Krim, M.; Acerbi, F.; Capasso, M.; Paternoster, G.; Mazzi, A.; Gola, A.; Chen, J.; Auffray, E. Vacuum ultraviolet silicon photomultipliers applied to BaF_2 cross-luminescence detection for high-rate ultrafast timing applicaitons. *Phys. Med. Biol.* **2021**, *66* (11), 114002.
(35) Hu, C.; Xu, C.; Zhang, L.; Zhang, Q.; Zhu, R.-Y. Development of Yttrium-Doped BaF_2 Crystals for Future HEP Experiments. *IEEE Trans. Nucl. Sci.* **2019**, *66* (7), 1854−1860.
(36) Seliverstov, D. M.; Demidenko, A. A.; Garibin, E. A.; Gain, S. D.; Gusev, Y. I.; Fedorov, P. P.; Kosyanenko, S. V.; Mironov, I. A.; Osiko, V. V.; Rodnyi, P. A.; Smirnov, A. N.; Suvorov, V. M. New fast scintillators on the base of BaF_2 crystals with increased light yield of 0.9ns luminescence for TOF PET. *Nuclear Instruments and Methods in Physics Research Section A: Accelerators, Spectrometers, Detectors and Associated Equipment* **2012**, *695*, 369−372.
(37) Rodnyi, P. A.; Terekhin, M. A. Radiative Core-Valence Transitions in Alkali-Halide Crystals. *Physica Status Solidi b: Basis solid state physics* **1991**, *166* (1), 283−288.
(38) Kubota, S.; MacDonald, M.; Munro, I. H. Auger-free luminescence excitation spectra in CsCl and CsBr between 50 and 140 eV. *J. Lumin.* **1991**, *48*−*49* (2), 589−592.
(39) Kubato, S.; Ruan, J.-z.; Itoh, M.; Hashimoto, S.; Sakuragi, S. A new type of luminescence mechanism in large band-gap insulators: Proposal for fast scintillation materials. *Nucl. Instrum. Methods Phys. Res., Sect. A* **1990**, *289* (1−2), 253−260.
(40) Macdonald, M. A.; Mel'chakov, E. N.; Munro, I. H.; Rodnyi, P. A.; Voloshinovsky, A. S. Radiative core-valence transitions in $CsMgCl_3$ and $CsSrCl_3$. *J. Lumin.* **1995**, *65* (1), 19−23.
(41) Shpak, A. P.; Glike, O. A.; Dmitriev, A. G.; Rodnyi, P. A.; Voloshinovskii, A. S.; Pidzyrailo, S. M. Radiative core-valence transitions in wide-gap crystals. *J. Electron Spectrosc. Relat. Phenom.* **1994**, *68*, 335−338.
(42) Koshimizu, M.; Yahaba, N.; Haruki, R.; Nishikido, F.; Kishimoto, S.; Asai, K. Scintillation and luminescence properties of a single $CsCaCl_3$ crystal. *Opt. Mater.* **2014**, *36* (12), 1930−1933.
(43) Vanecek, V.; Paterek, J.; Kral, R.; Kucerkova, R.; Babin, V.; Rohlicek, J.; Cala, R.; Kratochwil, N.; Auffray, E.; Nikl, M. Ultraviolet cross-luminescence in ternary chlorides of alkali and alkaline-earth metals. *Opt. Mater.: X* **2021**, *12*, No. 100103.
(44) Rutstrom, D.; Stand, L.; Delzer, C.; Kapusta, M.; Glodo, J.; van Loef, E.; Shah, K.; Koschan, M.; Melcher, C. L.; Zhuravleva, M. Improved light yield and growth of large-volume ultrafast single crystal scintillators Cs_2ZnCl_4 and Cs_3ZnCl_5. *Opt. Mater.* **2022**, *133*, No. 112912.
(45) Rutstrom, D.; Stand, L.; Windsor, D.; Xu, H.; Kapusta, M.; Melcher, C. L.; Zhuravleva, M. New ultrafst scintillators with core valence luminescence: Cs_2MgCl_4 and Cs_3MgCl_5. *J. Mater. Chem. C* **2024**, *12*, 6920−6931.
(46) Takahashi, K.; Koshimizu, M.; Fujimoto, Y.; Yanagida, T.; Asai, K. Auger-free luminescence characteristics of $Cs(Ca_{1-x}Mg_x)Cl_3$, Nuclear Instruments and Methods in Physics Research Section A: Accelerators, Sopectrometers. *Detectors and Associated Equipment* **2020**, *954*, 161842.

https://doi.org/10.1021/acsaom.5c00253
ACS Appl. Opt. Mater. 2025, 3, 2101−2110

(47) Voloshinovskii, A. S.; Mikhailik, M. S.; Mikhailik, V. B.; Melçhakov, E. N.; Rodnyi, P. A.; van Eijk, C. W. E.; Zimmerer, G. Immpurity core-valence luminescence in $Rb_{1-x}Cs_xCl$ mixed crystals. *J. Lumin.* **1998**, *79* (12), 107−114.
(48) Voloshinovskii, A. S.; Mikhailik, V. B.; Rodnyi, P. A. Impurity-induced core-valence lumionescence: A new possibility for fast scintillators creation. *Radiat. Meas.* **1995**, *24* (4), 383−385.
(49) Jansons, J. L.; Krumins, V. J.; Rachko, Z. A.; Valbis, J. A. Crossluminescence of KF and related compounds. *Solid State Commun.* **1988**, *67* (2), 183−185.
(50) Chornodolskyy, Ya; Stryganyuk, G.; Syrotyuk, S.; Voloshinovskii, A.; Rodnyi, P. Features of the core-valence luminescence and electron energy band structure of $A_{1-x}Cs_xCaCl_3$ (A = K, Rb) crystals. *J. Phys.: Condens. Matter* **2007**, *19* (47), No. 476211.
(51) Rutstrom, D.; Stand, L.; Kapusta, M.; Windsor, D.; Xu, H.; Melcher, C. L.; Zhuravleva, M. Impurity-enhanced core-valence luminescence via Zn-Doping in cesium magnesium chlorides. *Optical Materials: X* **2024**, *24*, No. 100349.
(52) Rutstrom, D. *Development of novel cesium chloride-based ultrafast inorganic scintillators for fast timing radiation detection applications*; PhD dissertation; University of Tennessee, 2024, https://trace.tennessee.edu/utk_graddiss/10161.
(53) Herweg, K.; Rutstrom, D.; Nadig, V.; Stand, L.; Melcher, C. L.; Zhuraavleva, M.; Schulz, V.; Gundacker, S. Timing limits of ultrafast cross-luminescence emission in CsZnCl-based crystals for TOF-CT and TOF-PET. *EJNMMI Phys.* **2024**, *11*, 59.
(54) Rossignol, J.; Martinez Turtos, R.; Gundacker, S.; Gaudreault, D.; Auffray, E.; Lecoq, P.; Berebu-Lauziere, Y.; Fontaine, R. Time-of-flight computed tomography - proof of principle. *Phys. Med. Biol.* **2020**, *65* (8), No. 085013.
(55) Dorenbos, P.; de Haas, J. T. M.; van Eijk, C. W. E. Non-Proportionality in the Scintillation Response and the Energy Resoluton Obtainable with Scintillation Crystals. *IEEE Trans. Nucl. Sci.* **1995**, *42* (6), 2190−2202.
(56) Khodyuk, I. V.; Dorenbos, P. Trends and Patters of scintillator Nonproportionality. *IEEE Trans. Nucl. Sci.* **2012**, *59* (6), 3320−3331.
(57) Khodyuk, I. V. *Nonproportionality of inorganic scintillators*, ISBN:9789088915536.
(58) Yahaba, N.; Koshimizu, M.; Sun, Y.; Yanagida, T.; Fujimoto, Y.; Haruki, R.; Nishikido, F.; Kishimoto, S.; Asai, K. X-ay detection capability of a Cs_2ZnCl_4 single crystal scintillator. *Appl. Phys. Express* **2014**, *7* (6), No. 062602.
(59) Takahashi, K.; Arai, M.; Koshimizu, M.; Fujimoto, Y.; Yanagida, T.; Asai, K. Luminescence and Scintillation Properties of Cs_2ZnCl_4 and Cs_3ZnCl_5. *Jpn. J. Appl. Phys.* **2020**, *59* (7), No. 072002.
(60) Ohnishi, A.; Kitaura, M.; Otoma, T.; Sasaki, M. Reflection spectrum and auger-free luminescence in molecular ionic crystals of Cs_2ZnCl_4. *J. Phys. Soc. Jpn.* **2003**, *72*, 2400−2401.
(61) Shi, C.-S.; Klaiber, T.; Zimmerer, G. Special luminescence properties of BaF_2 crystals. *J. Lumin.* **1988**, *40*−*41*, 189−190.
(62) Shi, C.-S.; Klaiber, T.; Zimmerer, G. Temperature effect of the luminescence bad at 300 nm from BaF_2 crystals. *J. Lumin.* **1991**, *48*−*49*, 597−600.
(63) Wolszczak, W.; Dorenbos, P. Time-resolved gamma spectroscopy of single events. *Nucear Instruments and Methods in Physics Research Section A: Accelerators, Spectrometers, Detectors and Associated Equipment* **2018**, *886*, 30−35.
(64) Kimura, K.; Wada, J. Excitaton-density-dependent competition between radiative and nonradiative annihilations of core holes produced by ion irradiation of a single-crystalline BaF_2. *Phys. Rev. B* **1993**, *48*, No. 15535.
(65) Novotny, R.; Beck, R.; Doring, W.; Hejny, V.; Hoek, M.; Hofstaetter, A.; Metag, V.; Romer, K. Scintillators for photon detection at medium energies - a comperative study of BaF_2, CeF_3 and $PbWO_4$. *Nucear Instrumetns and Methods in Physics Research Section A: Accelerators, Spectrometers, Detectors and Associated Equipment* **2002**, *486* (1−2), 131−135.
(66) Lushchik, C. B.; Savikhin, F. A.; Makhov, V. N.; Ryabukhin, O. V.; Ivanov, V. Y.; Kruzshalov, A. V.; Neshov, F. G. Recombination-assisted creation of cation excitons and cross-luminescence quenching in CsCl crystals at high excitation densities. *Phys. Solid State* **2000**, *42*, 1052−1057.
(67) Rodnyi, P. A.; Mikhailik, V. B.; Stryganyuk, G. B.; Voloshinovskii, A. S.; van Eijk, C. W. E.; Zimmerer, G. F. Luminescence properties of Ce-doped $Cs_2LiLaCl_6$ crystals. *J. Lumin.* **2000**, *86* (2), 161−166.
(68) van Loef, E. V. D.; Dorenbos, P.; van Eijk, C. W. E.; Kramer, K. W.; Gudel, H. U. Scintillation and spectroscopy of the pure and Ce^{3+}-doped elpasolites: Cs_2LiYX_6 (X = Cl, Br). *J. Phys.: Condens. Matter* **2002**, *14*, 8481.
(69) Yoshida, H.; Hayashi, M.; Itoh, M. Intensity enhancement of auger-free luminescence in BaF_2 and CsCl by acceleration voltage of electron-beam excitation. *Jpn. J. Appl. Phys.* **2000**, *39*, No. L215.
(70) de Haas, J. T. M.; Dorenbos, P. Advances in Yield Calibration of Scintillators. *IEEE Trans. Nucl. Sci.* **2008**, *55* (3), 1086−1092.

https://doi.org/10.1021/acsaom.5c00253
ACS Appl. Opt. Mater. 2025, 3, 2101−2110